European Journal of Pharmaceutical Sciences 221 (2026) 107498

Contents lists available at ScienceDirect

European Journal of Pharmaceutical Sciences

journal homepage: www.elsevier.com/locate/ejps

Computational modeling of the early-stage solubilization of a fenofibrate aggregate into mixed bile salt and fatty acids micelles

Fatmegyul Mustan [a,*], Anela Ivanova [b], Slavka Tcholakova [a]

[a] Department of Chemical and Pharmaceutical Engineering, Faculty of Chemistry and Pharmacy, Sofia University, Bulgaria
[b] Department of Physical Chemistry, Faculty of Chemistry and Pharmacy, Sofia University, 1 James Bourchier Ave., 1164 Sofia, Bulgaria

ARTICLE INFO

Keywords:
Drug solubilization
Fenofibrate
Taurodeoxycholate
Fatty acids
All-atom molecular dynamics
Lipid-based formulations

ABSTRACT

The behavior of a fenofibrate aggregate in water and its interaction with pure sodium taurodeoxycholate (TDC) micelles, as well as with mixed micelles of TDC and fatty acids (myristic, oleic, and stearic), was studied using atomistic molecular dynamics simulations. For each system, 500 ns trajectories were generated and analyzed in terms of the association of amphiphiles around the drug aggregate and their impact on the morphology and intermolecular interactions of the drug molecules. The results show that in the absence of fatty acids TDC covers the surface of the drug aggregate, shielding it from water without disrupting its structure. In contrast, all studied fatty acids intercalate between the drug molecules in the aggregate. However, myristic and stearic acids do not shield sufficiently the drug molecules from water, while oleic acid significantly reduces the contact between water and drug molecules. Two key requirements for effective solubilization are identified: (1) the ability of amphiphiles to disrupt the nanostructure of the drug aggregate, and (2) the flexibility and capability of amphiphiles to reduce interactions between water and hydrophobic drug molecules. These requirements were used to evaluate the efficiency of fatty acids in increasing the solubilization capacity of TDC micelles. A very good correlation was established between the efficiency determined from molecular dynamics simulations and experimental data known from the literature. The methodology developed in this study could be widely used to compare the efficiency of new lipid-based drug delivery formulations to solubilize hydrophobic drug molecules.

1. Introduction

Most of the active pharmaceutical ingredients (API) are provided as tablets for oral administration. The subsequent dissolution and absorption of the introduced molecules take place in the gastrointestinal tract (GI) (Pouton et al. 2006). Usually, these APIs are poorly water-soluble and hence are being often solubilized into the mixed micelles of bile salts and lipids formed in the intestinal fluids (Dressman and Reppas, 2000). The solubilization process is crucial for the following absorption and action of the administered drug in the human body. Therefore, the ability to control the bioactivity requires knowledge of the separate stages. However, there are many processes taking place when the drug molecules pass through the GI and many factors need to be considered. Although the solubilization step has been studied extensively, there are still knowledge gaps, especially at the molecular level. In the last decade, *in silico* studies are intensively used in the drug design and development (Guruge et al., 2023) but still microscopic understanding of the drug solubilization is lacking.

Usually, the key players in the solubilization of poorly water-soluble drugs are the bile salts by forming mixed micelles with phospholipids and free fatty acids (Katev et al., 2021) which are among the main products of triglyceride lipolysis during digestion (Mu and Hoy, 2004). As a result of the latter, phospholipid and fatty acid molecules appear mainly as monomers in the GI fluid, which then associate with existing bile salt micelles to form mixed micelles. The solubilization capacity of the mixed micelles depends on their specific composition, making it essential to study their behavior in detail to understand the mechanism of the process (Phan et al., 2015). Before studying the solubilization process itself, it is important to know well the behavior and properties of the micelles formed in the intestinal fluid. Previously, we studied the aggregation behavior of taurodeoxycholate (TDC) as a representative of bile salts and its mixed micelles with fatty acids (FA) with different hydrocarbon chain length (C14 and C18) and saturation (C18:0 and C18:1) (Mustan et al., 2024). It was shown that all studied fatty acids formed mixed micelles with taurodeoxycholate or solubilized into its micelles, depending on the nature of the hydrocarbon tail. The saturated

* Corresponding author.
E-mail address: fm@lcpe.uni-sofia.bg (F. Mustan).

https://doi.org/10.1016/j.ejps.2026.107498
Received 9 January 2026; Received in revised form 23 February 2026; Accepted 9 March 2026
Available online 10 March 2026

chains were mainly solubilized, screening their hydrophobic tails from the aqueous media. In contrast, the unsaturated tail, being much more flexible than the saturated ones, was well homogenized with TDC, forming mixed micelles with fluid hydrophobic core, which could be very welcoming media for poorly water-soluble substances. The same behavior of the unsaturated long tails was observed in coarse-grained molecular dynamics (MD) simulations (Tuncer and Bayramoglu, 2022). Unlike, the saturated FA created a more tightly ordered core, especially C18:0, which solidified at the studied temperature of 37 °C. Experimentally, significant impact of the hydrocarbon chain of fatty acids (Hofmann and Hagey, 2014; Malik, 2016; Pavlovic et al., 2018) and glucosides (Srivastava et al., 2026) on the solubilization of different poorly water-soluble drug molecules was registered, too. In a subsequent paper, we studied the solubilization of single molecules of six different drugs into mixed taurocholate/phospholipid micelles by using a single micelle and a drug monomer to estimate the complete solubilization (Mustan et al., 2025). For the first time, quantitative correlation between the experiment and MD simulations regarding solubilization was obtained.

Comparison with literature data showed that most of the solubilization studies available in the literature report molecular models containing monomers of the drug as well (Kabedev et al., 2021; Parrow et al., 2023). However, upon oral administration of the API, it does not reach the intestines as monomers well dissolved in the aqueous phase. Instead, it is in amorphous phase, which needs to be disrupted, and then the released molecules are solubilized and transferred to the membrane. Along these lines, primarily amorphous solid dispersions of APIs are studied by MD simulations regarding their stability and the role of proteins in this process (Brunsteiner et al., 2018; Barmpalexis et al. 2019; Xiang and Anderson, 2013). The solubilization of a drug aggregate into bile salt micelles was also studied in the context of transport mechanisms of danazol to lipid bilayers (Kabedev et al., 2021). It was found that bile salt micelles (composed of taurocholate and phospholipids) formed in the intestinal fluid might act as drug delivery shuttles and facilitate drug incorporation into cellular membranes. The process was studied for a monomer (by all-atom simulations) and an aggregate (composed of 10 molecules, by coarse-grain simulations) of API and their solubilization was observed. The potential of mean force was estimated from umbrella-sampling simulations where danazol was pulled from the micelle and from the membrane to the water phase. The obtained data suggest that in both cases the energetically favorable states are when the drug is solubilized mostly in the membrane and not in the micelle. However, in this study the focus is on the transportation of the API and the mechanism of its solubilization into the bile salt micelles is not discussed in detail.

So far, little attention has been paidto the initial stage of solubilization, when the nanostructure of the API first comes into contact with intestinal micelles. Having already characterized one variation of intestinal micelles in our previous work (Mustan et al., 2024), the natural next step was to investigate their solubilization capacity explicitly in the presence of an aggregate of drug molecules. This upgrades our previous work of monomers solubilization by bringing the methodology closer to experiment. In this context, the main goal of the present study is to clarify the role of fatty acids - specifically their hydrocarbon chain length and degree of saturation - in mixed micelles with bile salt during the early stage of drug solubilization when the drug molecules are arranged in a nanoaggregate.

2. Molecular models and computational protocol

2.1. Molecular models

Four systems are built and simulated by fully atomistic MD in explicit aqueous medium, containing an amorphous aggregate of fenofibrate (Tricor) (abbreviated as FFB in the text) in the presence of 1) TDC (abbreviated as TF in the text); 2) TDC + C14:0 (abbreviated as TMF in the text); 3) TDC + C18:0 (abbreviated as TSF in the text); or 4) TDC + C18:1 (abbreviated as TOF in the text). The FFB aggregate was spontaneously obtained in a separate simulation at high concentration of monomers in a small cubic box of 5 nm edge length for 2 ns. All acids are deprotonated and neutralized with sodium cations. The chemical structures of the used molecules are presented in Table 1. The model systems for the simulations are constructed in such a way as to mimic as closely as computationally feasible the experimental conditions of in vitro experiments (Katev et al., 2021). Following the same procedure for solution preparation, we constructed the model systems in the same order of addition of the components: (1) preparation of a TDC solution containing pure TDC micelles by running a separate simulation with the desired amount of TDC as monomers for 200 ns (Mustan et al., 2024); (2) addition of an FFB aggregate; this corresponds to the FFB powder added to the TDC solution in the experiment; (3) addition of excipient, i.e. fatty acids, as monomers, again similar to experiment. The concentrations of the main components are 50 mM TDC and FAs and 20 mM FFB. The electrolytes concentration is 137 mM NaCl and 10 mM KCl. The ratio between TDC and FAs is 1:1 as it is in the experiment. These concentrations of the components correspond to 100 TDC and 100 FA (Table 1) anions neutralized with 200 Na^+, and the electrolytes 278 NaCl and 20 KCl added as ions in the aqueous solutions. This results in models with ca. 103,500 water molecules in a cubic periodic box with edge length of 15 nm, giving ca. 325×10^3 atoms in total. All molecules/aggregates/ions are inserted at random into the simulation box. The initial configurations are presented in Figs. 1 and **S1** in the Supporting information (SI). All simulations are run for 500 ns and the last 100 ns are used for analysis. Additional simulation of the pure drug aggregate was run for 100 ns for its characterization. Note that when preassembled drug molecules are discussed, with or without associated TDC and/or fatty acid molecules, they are referred to as aggregates; in contrast, structures composed solely of assembled amphiphiles containing TDC are described as micelles.

2.2. Computational protocol

The structures of TDC, FA, FFB and electrolytes are described with the force field AMBER99 (Cornell et al., 1995), and the model TIP3P (Jorgensen et al., 1983) is used for the water. The force field parameters for TDC, FA, and FFB were derived in our previous works (Mustan et al., 2024; Hofmann et al., 2014, 2025), where the accuracy of the models was verified extensively against experimental data for these compounds. The existing optimized geometry files are directly used for the construction of the systems studied in this work. The current parameterization protocol includes the following steps: i) conformational search with AMBER99 in water and geometry optimization of the representative structures with the DFT functional B3LYP (Becke, 1988, 1993) and basis set 6–31G* (Ditchfield et al., 1971) *in vacuo*; ii) calculation of the atomic partial charges by applying the RESP (Restrained ElectroStatic Potential) procedure (Bayly et al., 1993; Cieplak et al., 1995), where the charges are fit to the quantum mechanical electrostatic potential of each molecule, generated at the HF/6–31G* level and the final RESP charges are averaged over the set of most stable conformers of each molecule; iii) import of the molecules into the force field library.

The following computational protocol was employed for all systems: *i*) energy minimization with the algorithm L-BFGS (Zhu et al., 1997); *ii*) heating to 310 K in NVT ensemble with Berendsen thermostat with coupling time of 0.1 ps (Berendsen et al. 1984); *iii*) relaxation for 1 ns in NVT ensemble at 310 K; *iv*) production runs for 500 ns with time step 2 fs in NVT ensemble. Note, the Berendsen thermostat was chosen for the heating phase for back-compatibility and comparability with our previous works on the topic where it was shown that the thermostat provides efficient and stable temperature control and reproduces the experimental behavior of the molecules (Mustan et al., 2015, 2024). In an independent work with a similar molecular system, we have studied the effect of thermostat and no influence was found in the molecular

Table 1
Composition of the molecular models.

Molecule	Abbreviation in the text	Chemical structure	Molar mass, g/mol	*C*, mM	Number of molecules
Fenofibrate	FFB	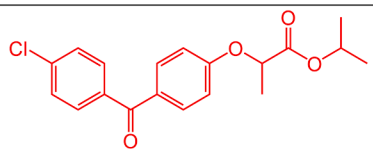	361	20	40
Taurodeoxycholate	TDC	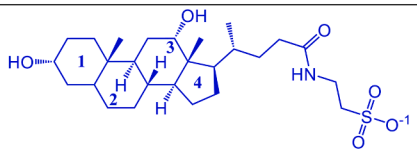	499	50	100
Myristate	C14:0		227	50	100
Stearate	C18:0		284	50	100
Oleate	C18:1		282	50	100

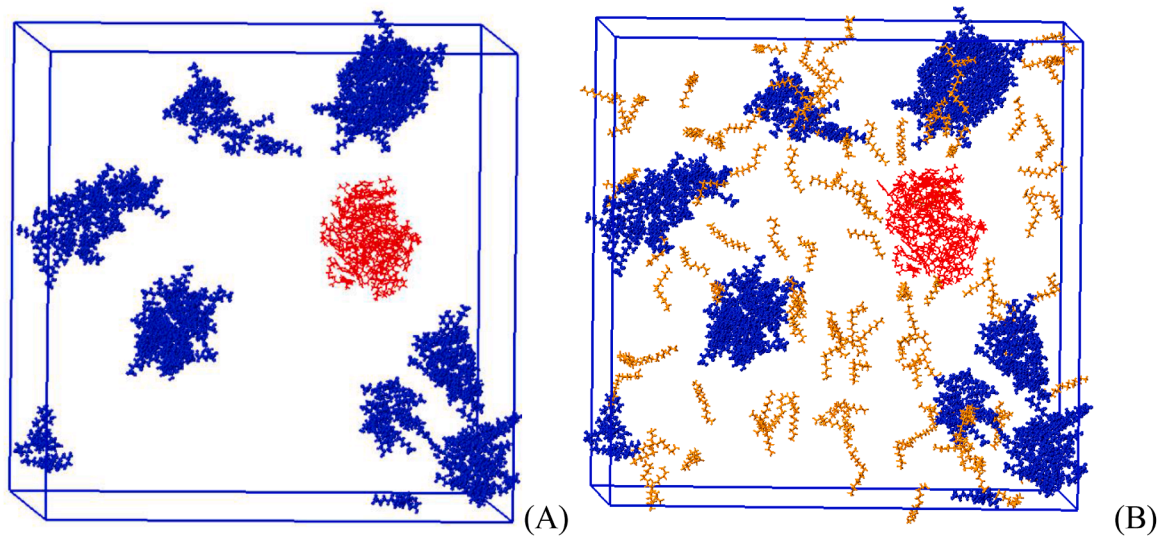

Fig. 1. Initial configuration of the systems containing (A) TDC (blue) + FFB (red), abbreviated as TF in the text, and (B) TDC (blue) + C14:0 (orange) + FFB (red), denoted as TMF. The configurations with C18:0 and C18:1 are identical to that with C14:0 and are illustrated in **Figure S1** in the SI. The water molecules and electrolytes ions are not visualized for clarity.

behavior under the applied conditions (Mustan et al., 2025). Snapshots were saved in the trajectories at intervals of 5 ps. The algorithm leapfrog (Hockney et al., 1974) was used to integrate the equations of motion during heating, relaxation and production runs. The lengths of all hydrogen-containing bonds were constrained with LINCS (Ryckaert et al., 1977) for the TDC, FA, and FFB and SETTLE for the water molecules (Miyamoto et al. 1992). The non-bonded interactions were described by a Lennard-Jones potential and a Coulomb term at cutoff 12 Å with a switch function initiated at 10 Å. The switch function accounts for this physical behavior by gradually reducing the interaction energies between 10 and 12 Å, ensuring a smooth transition to zero at the cutoff distance. This improves accuracy by ensuring forces and potentials are continuous and differentiable, preventing artifacts. The particular values were selected to correspond to those used in the derivation and validation of the used force field. Long-range electrostatic interactions were evaluated with the PME method (Darden et al., 1993; Essmann et al., 1995). The GROMACS 2021.3 software package (Lindahl et al., 2021) was used for all simulations and analysis, whereas VMD was

employed for visualization of the trajectories (Humphrey et al., 1996).

3. Results and discussion

3.1. Composition of the drug aggregate

The obtained trajectories were analyzed with respect to the number and size of micelles formed in the simulation box (**Figure S2** in the SI). However, only the drug-containing aggregate was examined in greater detail. In all systems, TDC and FA molecules were found to be adsorbed on the surface of the drug aggregate, and in no case was separation of FFB molecules from the aggregate observed. Typically, the dissolution of lipophilic drugs occurs over significantly longer timescales (of the order of hours) than those accessible in atomistic simulations. In this study, the experimental conditions were mimicked in terms of system composition and sequence of addition of components but not in terms of timescale, as experimental solubilization involves mixing for up to 24 h. Such long timescales remain inaccessible even to coarse-grained or mesoscopic simulations. Lack of dissociation of single molecules from the aggregate was registered even over the course of 2 μs all-atom and coarse-grain simulations (Kabedev et al., 2021). Therefore, the focus of the current study is on the initial stages of solubilization and the role of excipients, rather than on the complete dissolution of the drug molecules. A detailed atomistic investigation of drug solubilization would require a different initial molecular configuration, which has been addressed in a separate study on similar systems (Mustan et al., 2025).

The systems reach a steady state during the simulations, as indicated by multiple trajectory analyses. One of the main criteria for selecting the simulation time was the evolution of the number of molecules adsorbed onto the drug aggregates. It reaches a constant value after approximately 100 ns, as shown in **Figure S3B** in the SI. In addition, the root mean square deviation (RMSD) as a function of simulation time was calculated and is presented in **Figure S3A** in the SI. The RMSD reaches steady-state behavior after about 300 ns for all studied systems, indicating structural equilibration. Based on these observations, the selected simulation times for the analysis in the range of 400–500 ns are sufficient to ensure that the systems are equilibrated and representative steady-state behavior is achieved. Only drug molecules and associated amphiphiles to the drug aggregate were then extracted to generate separate trajectories for further detailed analysis. Two independent simulations were analyzed by the same way and average values with corresponding standard deviations were calculated.

It was found that in the absence of fatty acids 28±10 TDC molecules were adsorbed onto the drug aggregate. In contrast, when fatty acids were present, the number of associated TDC molecules was significantly reduced to 16±10 in the presence of C14:0, to 10±4 in the presence of C18:0, and to 12±6 in the presence of C18:1 (Table 2). This reduction is attributed to the solubilization of fatty acids within TDC micelles formed in the bulk away from the drug aggregate (**Figure S2** in the SI). Mechanistically, this effect arises from competitive interactions: both FFB and FA molecules seek to associate with the bile salt micelles to minimize their exposure to water. As a result, some bile salt molecules are engaged in solubilizing FA in the bulk, reducing their availability to interact with the drug aggregate. This explanation provides a molecular-level understanding of the redistribution of bile salts in the system. Also, the formation of isolated pure fatty acid micelles was observed in all systems (**Figure S2** in the SI). This behavior arises from the limited solubility of fatty acids, even in biorelevant media rather than water, which leads to their partial precipitation in experiments (Katev et al., 2021). However, delving deeper into this mechanism falls outside the scope of the study. The number of fatty acid molecules associated with the drug aggregate is 41±3 C14:0, 21±1 C18:0, and 23±1 C18:1. In cases where a property depends on the number of associated molecules, it has been appropriately normalized to enable direct comparison between the different systems.

Table 2
Composition of the largest aggregates at 500 ns averaged from two independent simulations.

System	Abbreviation	Number of molecules in the aggregate			Concentration corresponding to the number of molecules, mmol/l	
		TDC	FA	FFB	TDC	FA
TDC + FFB	**TF**	**28 ± 10**	**-**	**40**	**13.8 ± 4.9**	**-**
TDC + Myristate + FFB	**TMF**	**9 ± 3**	**41 ± 3**	**40**	**7.9 ± 4.9**	**19.9 ± 1.2**
TDC + Stearate + FFB	**TSF**	**10 ± 4**	**21 ± 1**	**40**	**4.9 ± 2.0**	**10.3 ± 0.5**
TDC + Oleate + FFB	**TOF**	**12 ± 6**	**23 ± 1**	**40**	**5.7 ± 2.7**	**11.1 ± 0.2**

It was particularly interesting to observe how the drug aggregate changed upon association with other molecules. To illustrate these changes, representative snapshots from the final simulation step are presented: in the absence of fatty acids (Fig. 2) and in their presence (Fig. 3). To visualize better the structural modifications, the initial structure of the drug aggregate - used to construct the model systems (Fig. 2**A**) - is compared with the modified aggregate, excluding visualization of the associated molecules (Fig. 2**B** - in the presence of TDC and Fig. 3 - in the presence of FA). Initially, the drug aggregate appears tightly packed (Fig. 2**A**), whereas its structure becomes looser upon interaction with other molecules, primarily due to the penetration of FA molecules among the drug molecules (Fig. 3). This is confirmed when visualizing the FA and TDC molecules in Fig. 3, which are visibly interspersed among the drug entities. Note, to avoid replicas, snapshot of the initial drug aggregate used in all systems is presented in Fig. 2**A.**

3.2. Morphology of the drug aggregate

The structural changes of the aggregate are quantified using radial distribution functions (RDFs) between fenofibrate molecules (Fig. 4**A**). In the pure drug aggregate, the FFB-FFB RDF exhibits a somewhat sharp, intense, and narrow peak, indicative of a well-ordered and tightly packed structure. In the presence of TDC alone, the RDF becomes more complex, showing multiple smaller peaks, although the first peak remains prominent. This suggests partial disruption of the aggregate structure, with some regions maintaining their compact packing. Snapshots confirm that TDC molecules are predominantly adsorbed onto the aggregate surface, forming a shell-like structure (Fig. 2**C**), while the core remains relatively intact. The well-preserved first RDF peak in the presence of TDC is attributed to these core drug molecules.

In the case of stearate, the RDF still shows a distinct peak, followed by a broad shoulder, but its intensity is lower. This case is unique due to the observed freezing of stearate tails, which form highly ordered, straight structures (Fig. 3**B** and **Figure S2C** in the SI), consistent with the high melting point (>37 °C) of stearate (Katev et al., 2021). This crystalline-like behavior is further confirmed by the RDF between stearate tails, which displays a sharp, narrow peak, characteristic of a well-ordered system (Fig. 4**B**, yellow line). Experimental data also indicate that stearate does not enhance fenofibrate solubilization under physiological conditions, as it precipitates due to its high melting point (Katev et al., 2021). In simulations, which use periodic boundary conditions and thus lack a container bottom, precipitation cannot occur as in experiments. Instead, formation of pure C18:0 nanocrystals is observed within the bulk, inside TDC micelles, and even inside the drug aggregate itself (**Figure S2C** in the SI).

For shorter-chain and unsaturated fatty acids, the RDF peaks for the FFB-FFB interactions are broader, a feature characteristic of fluid-like structures (Fig. 4**B).** This indicates that these FAs more efficiently disrupt the ordered packing of the drug aggregate. Snapshot analyses

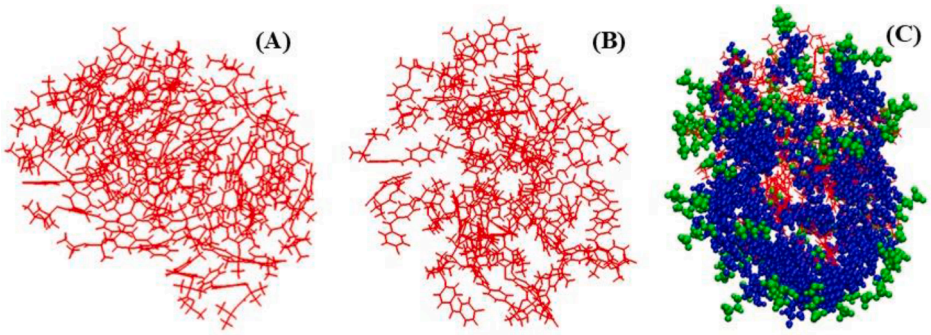

Fig. 2. Snapshots of (A) the initial aggregate of fenofibrate (Tricor) - red lines used for construction of the systems with TDC and FA, (B) the FFB aggregate at the end of the simulation in the presence of TDC, and (C) the same aggregate as (B) with visualized TDC molecules (blue balls - steroid skeleton, green balls - taurine residue) spontaneously associated around the drug aggregate after 500 ns.

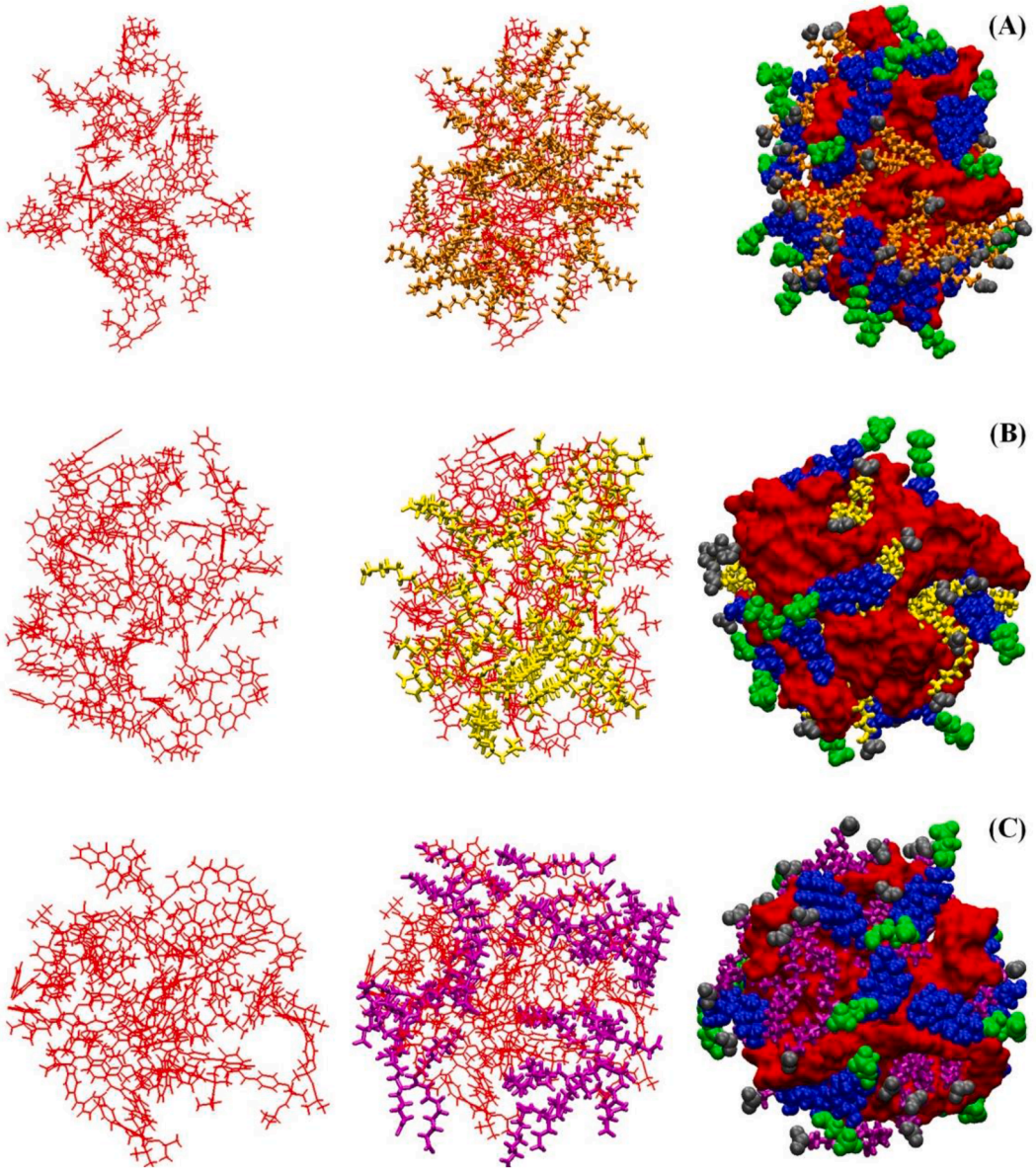

Fig. 3. Snapshots of FFB (red) aggregates at 500 ns in the systems with (A) C14:0 (orange tail and gray COO^-), (B) C18:0 (yellow tail and gray COO^-), and (C) C18:1 (purple tail and gray COO^-). The same aggregate in the particular system is illustrated from left to right by visualizing (left) only the FFB molecules, (middle) them with the associated FA molecules and (right) with TDC molecules (blue skeleton and green taurine residue). The structures obtained from the first series of simulations are used.

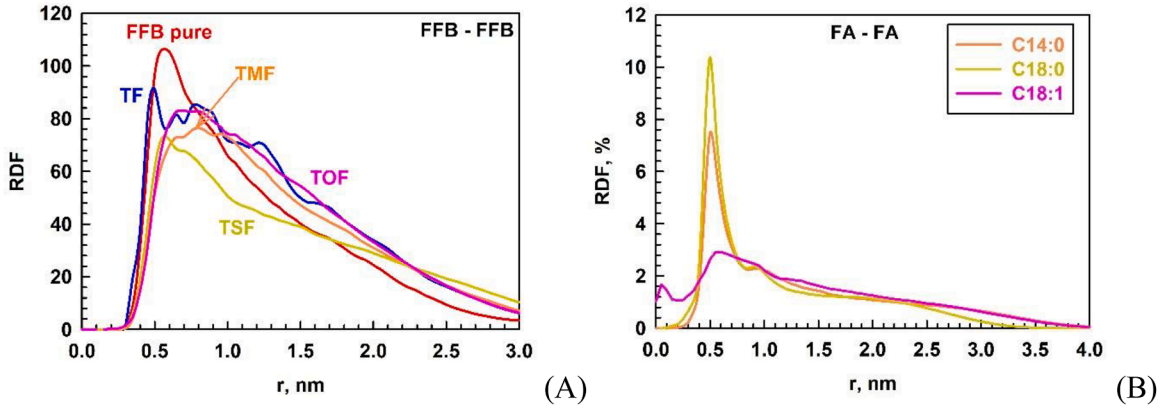

Fig. 4. RDF between the center of geometries of the (A) fenofibrate molecules and (B) fatty acids molecules in the systems without acids (red line), in the presence of TDC, TF (blue line), TDC + C14:0, TMF (orange line), TDC + C18:0, TSF (yellow line), TDC + C18:1, TOF (pink line).

also show that these molecules are homogeneously distributed within the aggregate, inserted between drug molecules (Fig. 3). Notably, in all FA-containing systems, TDC molecules consistently remain adsorbed on the aggregate surface, shielding some of the exposed drug molecules from water. Regarding the interactions between FA tails, the radial distribution function for the saturated C14:0 chain also exhibits a well-defined peak, similar to that of C18:0, though with lower intensity. In contrast, the RDF for unsaturated fatty acid tails is significantly lower in intensity and broader in shape compared to those of saturated chains. This behavior reflects the differing packing abilities of the molecules and was observed also in our previous work in the mixed micelles composed of TDC and various FAs (Mustan et al., 2024). There, it served as an indicator of the solid-like behavior of saturated tails and the fluid-like phase of unsaturated ones. The presence of a double bond in the middle of the C18:1 chain increases molecular flexibility and induces bending, which prevents the molecule from packing as densely as the saturated ones.

In addition to the visual analysis of the morphology of the obtained aggregates, inspection of the radial distribution functions of the whole molecules (Fig. 5) and of individual molecular fragments (**Figure S4** in the SI), relative to the geometrical center of the FFB aggregate, was performed. The respective cumulative functions are also plotted in **Figure S5** of the SI. It is observed that, except in the system with C18:0, the core of the aggregate is composed primarily of FFB molecules,

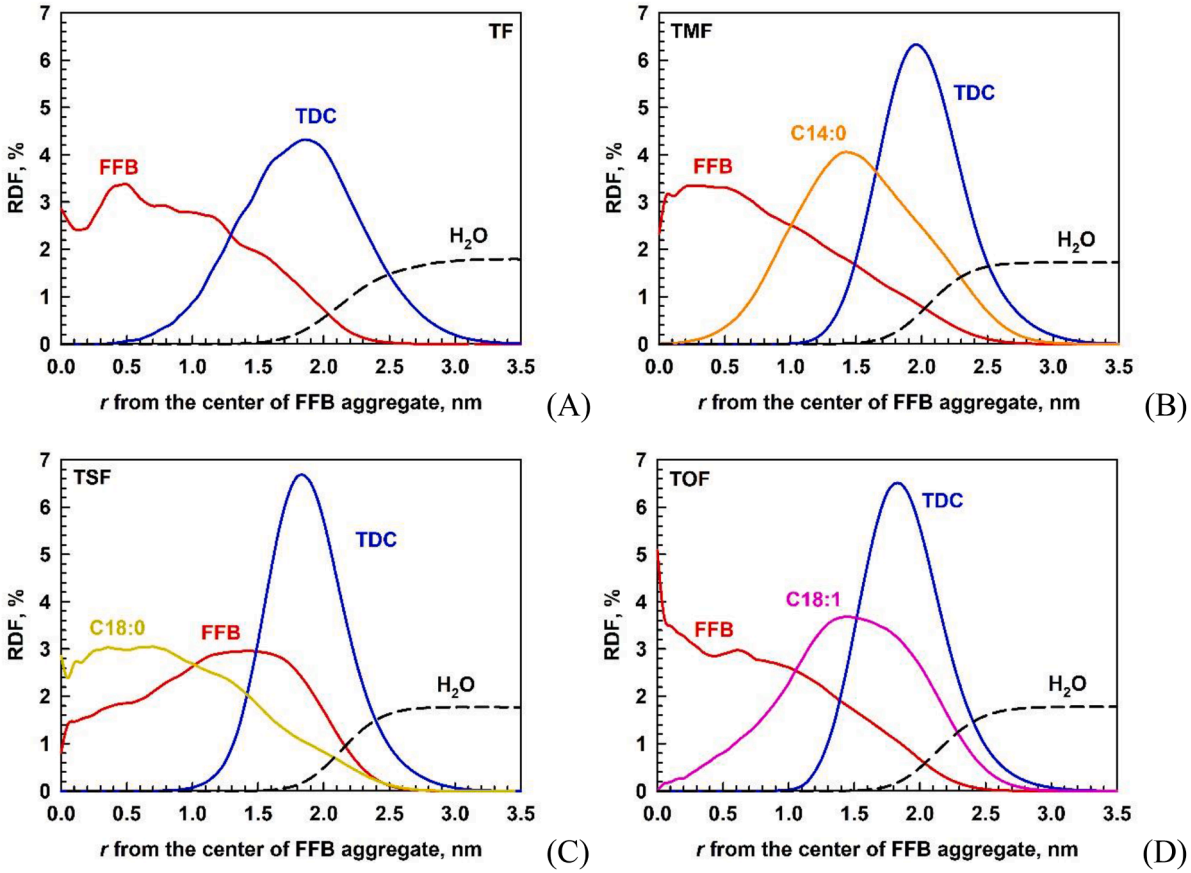

Fig. 5. Scaled RDFs calculated from the center of the FFB aggregates for each type of molecules in the systems: FFB - red, (A) TDC - blue, (B) C14:0 - orange, (C) C18:0 - yellow, and (D) C18:1 - pink; water - black dashed line.

followed by FA (when present), and TDC occupying the periphery of the aggregate, positioned between the hydrophobic core and the surrounding water.

In the absence of FA, the RDF peak of TDC is broader and begins at a distance of 0.5 nm from the center of the aggregate. In contrast, in the presence of FA, the TDC RDF peak becomes narrower and shifts outward, starting at approximately 1 nm. This suggests that in the absence of FA some TDC molecules penetrate into the drug aggregate, whereas in the presence of more hydrophobic excipients (FA), the acids preferentially occupy the interior and TDC molecules form a shell surrounding the structure. Notably, in all systems, the outer edge of the FFB RDF remains fixed at 2.5 nm (distance at the interface with water), indicating that the overall size of the aggregate does not change upon association with other molecules - only internal rearrangements occur.

The TDC RDF decays to zero at a slightly longer distance from the center than that of the other molecules. For all FA, the RDF begins to increase near the core of the aggregate. In the cases of C14:0 and C18:1, a well-defined peak is observed at approximately 1.3 - 1.4 nm. However, the RDF profile of C18:0 closely resembles that of FFB, with its highest values located even closer to the center of the aggregate than the drug itself. This observation is in excellent agreement with the visualized structures shown in Fig. 3**B**.

In all cases, a certain amount of water is in contact with the outmost FFB molecules located at the surface of the aggregate, but not with those in its core. The most hydrophilic fragments - the taurine tail of TDC and the carboxylate group of the FA - constitute the outermost parts of the aggregates and interact directly with the surrounding water (**Figure S4** in the SI).

3.3. *Properties of the aggregate: number of shielded FFB molecules and solvent-accessible surface area*

Using the radial distribution function, in this case calculated between each individual FFB molecule and all others, the number of neighboring molecules within a radius of 1.7 nm was determined. This threshold was selected based on the RDF calculated for the atoms within a single molecule, which corresponds to the maximum spatial extent of the FFB molecular structure during the simulations. This value is in good agreement with the 3D geometric descriptor of *maximum projection diameter, 1.9 nm,* calculated with Chemaxon© (chemaxon.com). Nevertheless, the effect of cutoff was studied in the range between 0.6 and 1.7 nm (**Figure S6** in the SI). At short cutoff values (up to ~1 nm), only the nearest-shell neighbors are captured, with counts varying between 1 and 4 per molecule. Increasing the cutoff to 1.7 nm incorporates additional layers of neighbors, which provides information about the overall packing and highlights the influence of amphiphiles on the rearrangement and disruption of the drug aggregate.

The following relation was used to calculate the number of neighbors of a certain FFB molecule:

$$N_{neighbor} = 4\pi\rho_{FFB}\int_{r=0}^{r=1.7} r^2 g_{FFB-FFB}\,dr \quad (1)$$

where $N_{neighbor}$ is the number of neighbors, ρ_{FFB} is the number density of the FFB molecules in the simulation box, $g_{FFB-FFB}$ is the RDF value between the single FFB and the rest of FFB molecules. $N_{neighbor}$ is calculated individually for all 40 FFB molecules and presented as a cumulative distribution function of the fraction of FFB molecules (Fig. 6). Alongside the systems containing bile salt and excipients, the same analysis was

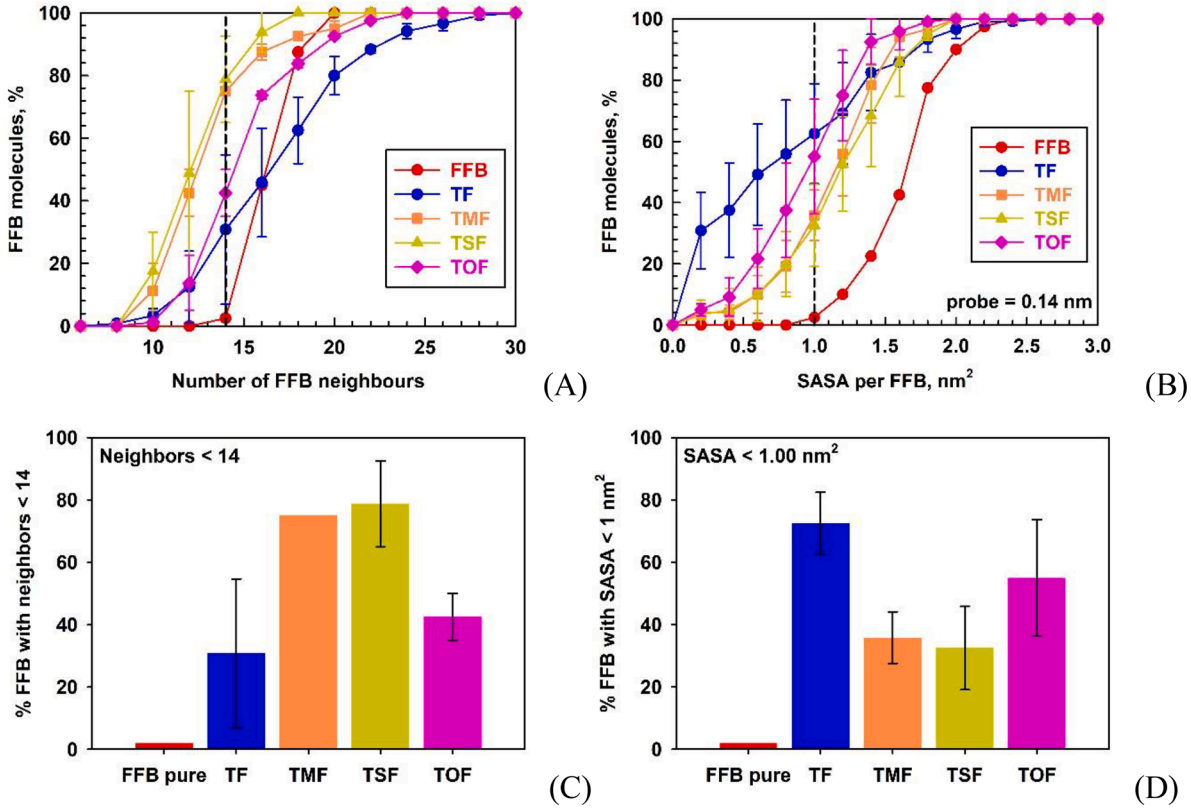

Fig. 6. Cumulative distribution of the percentage of FFB molecules as a function of (A) number of FFB neighbors and (B) SASA per FFB molecule in the systems of pure FFB (red curves), TF (blue curves), TMF (orange curves), TSF (yellow curves), and TOF (pink curves); the black lines denote the selected limiting values. Bar charts of the percentage of FFB molecules with (C) neighbors <14 and (D) SASA smaller than 1 nm^2. Averages and standard deviations from two independent trajectories for each system are shown.

carried out for a pure FFB aggregate obtained from a separate 100 ns MD simulation. In the bare aggregate, each FFB molecule interacts with at least 14 neighboring molecules within a 1.7 nm radius. However, the addition of bile salt significantly reduces this number: the minimum value drops from 14 to 9 neighbors, and the maximum increases to 25. This much broader range in the number of neighbors observed in the presence of TDC, compared to the pure aggregate, reflects the structural inhomogeneity introduced by TDC association. Some FFB molecules, located in the core, remain fully surrounded by other FFB molecules, whereas others are partially surrounded by TDC or even exposed to water. The degree of water accessibility to the aggregate is further assessed through the solvent-accessible surface area, which is discussed in the next section.

The addition of excipients follows the same trend of decreasing the number of FFB neighbors. This effect is most pronounced in the presence of C18:0, where the number of neighbors ranges between 8 and 16, indicating a substantial impact on the aggregate morphology. As previously noted, C18:0 is incorporated into the core (Fig. 5**C**) of the aggregate, forming a nanocrystalline structure that disrupts the tightly packed organization of the FFB molecules and significantly increases their exposure to water (Fig. 3**B**). In this case, both C18:0 and FFB, being highly hydrophobic, must be solubilized by TDC micelles. This competition contributes to the inefficacy of C18:0 as an excipient, as confirmed by experimental observations (Katev et al., 2021).

In the presence of C14:0, the minimum number of FFB neighbors is also 8, as observed with C18:0, but it increases up to 22. This indicates that the entire structure of the aggregate is not uniformly affected by the presence of C14:0. In contrast, in the presence of C18:1, the number of neighbors spans an even broader range (9 - 24), similar to that observed with TDC. Due to its bent structure, C18:1 is less capable of penetrating the aggregate core than saturated tails; nevertheless, it still disrupts the internal organization of the drug nanostructure. The profiles of the cumulative curves show that the saturated tails behave similarly to each other, whereas the profiles for C18:1 and TDC resemble one another (Fig. 6**A**).

To estimate the efficiency of each surfactant in disrupting molecular packing within the aggregate, the percentage of FFB molecules with <14 neighbors was calculated (Fig. 6**C**). In the pure aggregate, only 2 % of FFB molecules have <14 neighbors, indicating a tightly packed structure. Upon addition of TDC alone, this fraction increases to 62 %, reflecting disruption of the aggregate periphery, as TDC molecules do not penetrate its core (Fig. 5**A**). In the presence of C18:0, the aggregate becomes significantly loosened, with 92 % of FFB molecules having <14 neighbors, signifying that the structure is almost completely rearranged. For C14:0 and C18:1, the corresponding values are 75 % and 50 %, respectively. This clearly shows that oleate tails are less able to penetrate and alter the core structure of the aggregate compared to saturated fatty acid tails.

These results suggest that one of the key roles of excipients is to disrupt the structure of drug aggregates, making the FFB molecules more accessible for solubilization into the mixed micelles of gastrointestinal fluids, primarily composed of bile salts. A similar effect of sodium caprate mixed with taurocholate was reported for peptide drugs, where reduced peptide-peptide interactions took place due to enhanced micelle-peptide coupling (Hossain et al., 2023). It is evident that bile salts alone are not sufficiently effective in disintegrating the drug aggregate due to their bulky and rigid molecular structure. The unsaturated tail, while more flexible than both TDC and saturated fatty acid chains, is also bulkier than linear chains, which limits its penetration into the drug aggregate. Nevertheless, it is the most effective excipient studied here, as shown also by experimental data (Katev et al., 2021). This indicates that disruption of the aggregate structure alone is not sufficient to achieve high solubilization efficiency. It is also important to note that the drug aggregate used in the simulations is too large to be solubilized as a single particle. The drug concentration applied, consistent with the experimental setup, is in large excess, which typically leads to precipitation, as observed experimentally (Katev et al., 2021).

Solubilization is defined as the process of increasing the solubility of a poorly water-soluble substance through the use of surfactants, which facilitate the incorporation of the solute into micelles and shield it from water exposure (Mantri et al., 2017). That requires taking into account the contribution of the contacts between the drug molecules and water. To evaluate the role of excipients in this context, we calculated the solvent-accessible surface area (SASA) for each FFB molecule individually, using a probe radius of 0.14 nm, corresponding to the size of a water molecule. The analysis includes all molecules associated with the aggregate. The SASA data were processed analogously to the neighbor analysis, presented as a cumulative function of the fraction of the FFB molecules from the SASA per molecule. The same approach was applied to the pure aggregate, which serves as the reference system.

The average SASA of the molecules in the pure aggregate is found to be 1.62 nm^2, with a minimum value of approximately 1 nm^2. The addition of TDC and various excipients significantly reduces the SASA, bringing it below 1 nm^2 (Fig. 6**B**). A comparative analysis of the systems is presented in terms of their efficiency in decreasing the SASA of FFB molecules below the threshold value of 1 nm^2 (Fig. 6**D**). In the absence of surfactants, only 2 % of the molecules exhibit a SASA below this threshold. Upon addition of TDC, this fraction increases to 63 %, while the presence of C14:0 results in 46 %, C18:0 in 30 %, and C18:1 in 81 % of the molecules exhibiting reduced SASA.

Interestingly, this trend is opposite to that observed for the number of neighbors per molecule. Although C18:0 most significantly disrupts the aggregate structure, this occurs at the expense of increased water exposure of the FFB molecules. Remarkably, the introduction of a single double bond in the fatty acid chain (as in C18:1) fundamentally alters its contribution. Due to steric effects and the weaker hydrophobicity of oleate, a substantial proportion of its molecules remain outside the aggregate, effectively shielding the FFB molecules from the aqueous environment.

The obtained trend in the fraction of FFB molecules with reduced SASA in the presence of FA is in very good agreement with the experimental data (Katev et al., 2021) but the result for TDC does not align with the experiment, where it is with the lowest solubilization capacity. One of the main differences between the systems studied with the MD simulations is the number of the TDC molecules associated into the drug aggregate, which has notable impact on the SASA - the more the surfactant molecules, the lower the SASA of the drug molecules. There are 38 TDC molecules in the absence of FA, but in the presence of excipients this number is in the range of 11 and 17. Although small, there are still differences in the number of FA, too. That is why we normalized the data from Fig. 6**D**, taking into account the number of associated molecules, and calculated the efficiency of the excipients with respect to TDC performance using the following relations:

$$\begin{aligned} \textit{Normalized efficiency} &= \frac{f_{SASA\,TDC}}{f_{SASA\,TDC(+FA)}}(c_1 + c_2) \\ c_2 = \frac{N_{C14:0}}{N_{FA}} c_1 &= \frac{N_{TDC\ in\ TF}}{N_{TDC\ in\ TDC+FA}}, \end{aligned} \tag{2}$$

where $f_{SASA\,TDC}$ is the fraction of FFB molecules with SASA < 1 nm^2 in the presence of TDC only, $f_{SASA\,TDC(+FA)}$ is the fraction of FFB molecules with SASA < 1 nm^2 in the presence of TDC or TDC+FA, c_1 and c_2 are the correction coefficients taking into account the different numbers of TDC (c_1) and FA (c_2) associated into the FFB aggregate in the different systems. c_1 is the ratio between the number of TDC molecules associated to the FFB aggregate in the absence of FA and in the presence of FA, c_2 is the ratio between the number of C14:0 in the FFB aggregate and the number of the other FA (C18:0 and C18:1).

To estimate the efficiency of the excipients in the experiment, the solubilization ratio is calculated as the ratio between the concentration of the solubilized drug in the excipient-containing solution and in the system containing only bile (Katev et al., 2021). The values N measured

for the same systems as studied in the current work are presented in **Table S1** in the SI. Note, the concentrations of the components used in the experiment (10 mM bile and 10 mM FA) are very close to those obtained in the simulations, taking into account only the molecules included in the drug aggregate (Table 1). We used the experimental solubilization ratio to create a correlation plot with the calculated efficiency of the FA in the simulations, based on the same consideration (Fig. 7). An excellent correlation between the computed and the experimental data is evident. It reveals that even in the early stage of the solubilization process the efficiency of the used excipients is pronounced.

To assess the robustness of the developed efficiency calculation approach, additional simulations were performed to examine the influence of the initial system configuration and molecular assembly pathway. In the first test system, termed "all-monomers," TDC, FFB, and FA monomers were randomly placed in the simulation box. In the second test system, referred to as "mixed micelles + FFB aggregate," preassembled mixed TDC+C14:0 micelles were used, followed by the addition of an FFB aggregate. The "all-monomers" simulations were carried out for all FA-containing systems, whereas the "mixed micelles + FFB aggregate" setup was investigated only for the C14:0 system, chosen as a representative case with intermediate solubilization efficiency.

In the case of the "all-monomers" systems, mixed micelles containing all molecular components were formed, and the largest micelle was analyzed in terms of SASA and the number of neighboring FFB molecules (Table S2 in the SI). Snapshots of the analyzed micelles clearly illustrate a molecular arrangement similar to that observed in the original simulations discussed above (Figure S7 in the SI). In addition, the same trend in solubilization efficiency was obtained, showing a strong correlation ($R^2 = 0.87$) with the experimental solubilization ratio (Figure S8 in the SI).

The results were also reproduced when preassembled mixed TDC+C14:0 micelles were simulated in the presence of an FFB aggregate (Figures S9 and S10, Table S3 in the SI). The snapshots show an identical molecular organization, with C14 fatty acid chains penetrating between FFB molecules and disrupting the aggregate, while TDC molecules form a stabilizing shell at the surface. Notably, although the fatty acids were initially arranged in mixed micelles with TDC, association of these micelles with the drug aggregate was again observed. This process is governed by the same intermolecular interactions as in systems where fatty acids were initially present as monomers in the bulk. Only in the case of preassembled mixed micelles, a larger number of molecules associate with the FFB aggregate compared to the original systems, which is reflected in the SASA of FFB: the increased surface coverage leads to a greater number of FFB molecules exhibiting SASA values below 1 nm^2.

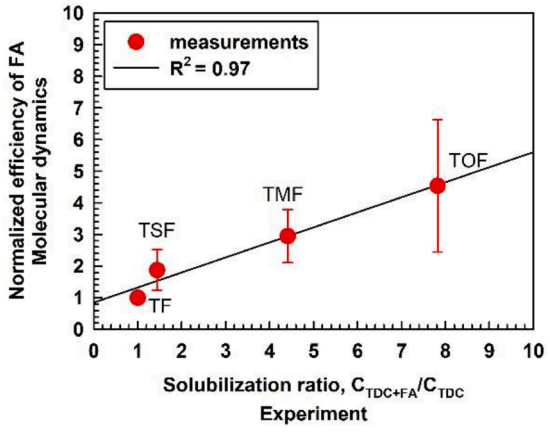

Fig. 7. Correlation plot between the calculated efficiency of the excipients in reducing the SASA of the FFB molecules and the experimentally measured solubilization ratio. Averages and standard deviations from two independent trajectories are shown.

The molecular-level insights obtained in this study have direct implications for the rational design of lipid-based pharmaceutical formulations for poorly water-soluble drugs. The simulations demonstrate that the solubilization efficiency of mixed bile salt-fatty acid micelles depends sensitively on both the chain length and the degree of saturation of the fatty acid excipient. Importantly, the results reveal that effective solubilization is not governed by a single factor but instead arises from a balance between drugaggregate disruption and shielding of drug molecules from aqueous exposure.

Previous molecular dynamics and experimental studies strongly support the trends observed in our simulations. Parrow et al. (Parrow et al., 2023; 2020) showed that bile salt-containing intestinal colloids dynamically reorganize in response to component composition, correlating with the solubilization of poorly water-soluble drugs. Birru et al. (Birru et al., 2017) used a four-component mixture (bile salt, lecithin, oleate, and monoglyceride at 11.7 mM total) to demonstrate that physiological surfactant ratios alter aggregate morphology and drug-micelle affinities through differences in lipophilicity, shape, and ionization - leading to orders-of-magnitude variations in solubility. Clulow et al. (Clulow et al., 2017) combined SANS, DLS, and MD to reveal heterogeneity in taurocholate-lecithin mixed micelles, ranging from spherical to elongated shapes, with bile salts locating preferentially at the surface and phospholipids - in the core; optimal ratios enhanced the drug-loading capacity of the hydrophobic core. Marrink at al. (Marrink et al., 2002) simulated phospholipid-bile salt systems, showing that bile salts localize at micelle surfaces, phospholipids in cores, and that increasing PC/BS ratios yields larger, more elongated shapes, while cholesterol increases micellar fluidity. Tuncer et al. (Tuncer et al., 2019) modelled taurodeoxycholate-fatty acid micelles, finding that longer fatty acid chains increase packing density and size, higher saturation enhances order and compactness, and bile salt identity affects hydrogen bonding and surface exposure. Together, these studies confirm that fatty acid chain length, degree of saturation, and bile salt identity are key determinants of aggregate size, packing, and surface exposure.

From a formulation perspective, these findings suggest that molecular dynamics simulations can be used as a predictive screening tool to evaluate excipient performance prior to experimental testing. In particular, the ability to assess how different lipid excipients interact with drug aggregates in the amorphous phase enables rapid comparison of candidate excipients and drug-excipient combinations. This approach is especially valuable for early-stage formulation development, where experimental screening may be limited by material availability or cost, and even for drug candidates that have not yet been synthesized.

The observed superior performance of unsaturated fatty acids, such as oleic acid, highlights the importance of molecular flexibility in enhancing solubilization. This insight provides a concrete design principle for selecting or engineering lipid excipients that maximize solubilization efficiency in mixed micellar systems. Overall, the results support the use of atomistic simulations as a practical tool for guiding excipient selection and optimizing lipid-based drug delivery systems.

4. Conclusions

Fully atomistic molecular dynamics simulations were conducted to investigate the influence of fatty acid chain length and degree of saturation on the interactions between an aggregate of 40 fenofibrate molecules and micelles of sodium taurodeoxycholate (TDC) in the absence and in the presence of fatty acids (myristic, stearic, or oleic). It was shown that a significant number of TDC molecules (28 ± 10 in total) adsorb onto the surface of the drug aggregate, effectively shielding it from water without markedly disrupting the core structure of the aggregate. This behavior is attributed to the amphiphilic nature of TDC, characterized by its planar steroidal skeleton.

All studied fatty acids were found to disrupt the drug aggregate by penetrating among fenofibrate molecules. This effect is most

pronounced for stearic acid, which however does not protect the drug molecules from water. Myristic acid also intercalates effectively between drug molecules in the aggregate, disrupts the tightly packed structure of the FFB aggregate and shields to some extent drug molecules from water. The unsaturated oleic acid exhibits dual functionality: it loosens the drug aggregate and significantly decreases the interactions between FFB and water molecules. This dual behavior is crucial for efficient solubilization and is attributed to its higher molecular flexibility compared to saturated analogs. This observation aligns with experimental data verifying highly enhanced solubilization of FFB in the presence of oleate as an excipient (Katev et al., 2021). The simulations show very good qualitative agreement with experimental observations of enhanced fenofibrate solubilization in the presence of oleate, validating the predictive value of the computational approach.

The revealed impact of lipid chain length and saturation on the solubilization capacity of mixed micelles composed of bile salts and fatty acids provides new insights into the mechanisms underlying the solubilization of poorly water-soluble drugs and the factors governing this process. Two key contributions are necessary for effective solubilization: (1) the ability of the surfactant to disrupt the drug nanostructure, making individual drug molecules more accessible to micelles; and (2) the flexibility and capability of the amphiphiles for effectively reducing the exposure of drug molecules to water. By linking molecular-scale behavior to macroscopic solubilization efficiency, this study demonstrates how atomistic simulations can support the rational design, screening, and optimization of lipid-based pharmaceutical formulations for poorly water-soluble drugs.

Funding

This study was funded by the European Union-NextGenerationEU, through the National Recovery and Resilience Plan of the Republic of Bulgaria, project No BG-RRP-2.004-0008.

Associated content

Supporting Information. The Supporting information contains 1) Initial configuration of the systems containing stearic and oleic acid (Figure S1), 2) Snapshots at 500 ns of the simulations of the systems and the aggregation numbers (Figure S2), 3) RMSD and number of molecules attached to the FFB aggregate as a function of simulation time (Figure S3), 4) Scaled RDFs calculated from the center of the FFB aggregates for two terminal fragments of each molecule (Figure S4), 5) Cumulative RDFs calculated from the center of the FFB aggregate for each component in the systems (Figure S5), 6) Number of FFB neighbors as a function of cutoff used for the calculations of the number of neighbors (Figure S6), 7) Cumulative distribution of the percentage of FFB molecules in the test simulations (Figure S7), 8) Experimental data for solubilization of fenofibrate (Table S1), 9) Composition of the biggest micelles formed in the simulations of the systems with initial configuration containing only monomers of all molecules (Table S2) or pre-assembled mixed micelles (Table S3).

CRediT authorship contribution statement

Fatmegyul Mustan: Writing – review & editing, Writing – original draft, Resources, Investigation, Formal analysis, Data curation. **Anela Ivanova:** Writing – review & editing, Supervision, Resources, Project administration, Methodology, Data curation, Conceptualization. **Slavka Tcholakova:** Writing – review & editing, Validation, Resources, Project administration, Conceptualization.

Declaration of competing interest

The authors declare that they have no known competing financial interests or personal relationships that could have appeared to influence the work reported in this paper.

Acknowledgements

We acknowledge the Discoverer PetaSC and EuroHPC JU for awarding access to Discoverer supercomputer resources located in Sofia, Bulgaria, and to the Operational Program “Science and Education for Smart Growth” under contract UNITe N^{o} BG05M2OP001-1.001-0004-C01 (2018-2023) for the allocated computational time.

Supplementary materials

Supplementary material associated with this article can be found, in the online version, at doi:10.1016/j.ejps.2026.107498.

Data availability

Data will be made available on request.

References

Barmpalexis, P., Karagianni, A., Katopodis, K., Vardaka, E., Kachrimanis, K., 2019. Molecular modelling and simulation of fusion-based amorphous drug dispersions in polymer/plasticizer blends. European J. Pharm. Sci. 130, 260–268. https://doi.org/10.1016/j.ejps.2019.02.004.

Bayly, C.I., Cieplak, P., Cornell, W.D., Kollman, P.A., 1993. A well behaved electrostatic potential based method uusing charge restraints for deriving atomic charges - the RESP model. J. Phys. Chem. 97, 10269–10280. https://doi.org/10.1021/j100142a004.

Becke, A.D., 1988. Density-functional exchange-energy approximation with correct asymptotic behavior. Phys. Rev. A: At. Mol. Opt. Phys. 38, 3098–3100. https://doi.org/10.1103/physreva.38.3098.

Becke, A.D., 1993. Density-functional thermochemistry. III. The role of exact exchange. J. Chem. Phys. 98, 5648–5652. https://doi.org/10.1063/1.464913.

Berendsen, H.J.C., Postma, J.P.M., van Gunsteren, W.F., DiNola, A., Haak, J.R., 1984. Molecular-dynamics with coupling to an external bath. J. Chem. Phys. 81 (8), 3684–3690. https://doi.org/10.1063/1.448118.

Birru, W.A., Warren, D.B., Han, S., Benameur, H., Porter, C.H.J., et al., 2017. Computational and experimental models of the gastrointestinal environment 2. Phase behavior and drug solubilization capacity of a type I lipid-based drug formulation after digestion. Mol. Pharmaceutics 14 (3), 580–592. https://doi.org/10.1021/acs.molpharmaceut.6b00887.

Brunsteiner, M., Khinast, J., Paudel, A., 2018. Relative contributions of solubility and mobility to the stability of amorphous solid dispersions of poorly soluble drugs: a molecular dynamics simulation study. Pharmaceutics 10, 101. https://doi.org/10.3390/pharmaceutics10030101.

Chemaxon: https://docs.chemaxon.com/display/docs/calculators_geometrical-descriptors-plugin.md.

Cieplak, P., Cornell, W.D., Bayly, C., Kollman, P.A., 1995. Application of the multimolecule and multiconformational RESP methodology to biopolymers - charge derivation for DNA, RNA, and proteins. *J. Comput. Chem.* 16, 1357–1377. https://doi.org/10.1002/jcc.540161106.

Clulow, A., Parrow, A., Hawley, A.M., Khan, J., Pham, A., et al., 2017. Characterization of solubilizing nanoaggregates present in different versions of simulated intestinal fluid. J. Phys. Chem. B 121 (48), 10869–10881. https://doi.org/10.1021/acs.jpcb.7b08622.

Cornell, W.D., Cieplak, P., Bayly, C.I., Gould, I.R., Merz, K., et al., 1995. A second generation force field for the simulation of proteins, nucleic acids, and organic molecules. J. Am. Chem. Soc. 117, 5179–5197. https://doi.org/10.1021/ja00124a002.

Darden, T., York, D., Pedersen, L., 1993. Particle mesh Ewald: an N·log(N) method for Ewald sums in large systems. J. Chem. Phys. 98, 10089–10092. https://doi.org/10.1063/1.464397.

Ditchfield, R., Hehre, W.J., Pople, J.A., 1971. Self-consistent molecular-orbital methods. IX. An extended gaussian-type basis for molecular-orbital studies of organic molecules. J. Chem. Phys. 54, 724–728. https://doi.org/10.1063/1.1674902.

Dressman, J.B., Reppas, C., 2000. In vitro-in vivo correlations for lipophilic, poorly water- oluble drugs. Eur. J. Pharm. Sci. 11, S73–S80. https://doi.org/10.1016/s0928-0987(00)00181-0.

Essmann, U., Perera, L., Berkowitz, M.L., Darden, T., Lee, H., Pedersen, L.G., 1995. A smooth particle mesh Ewald method. J. Chem. Phys. 103, 8577–8593. https://doi.org/10.1063/1.470117.

Guruge, A.G., Warren, D.B., Pouton, C.W., Chalmers, D.K., 2023. Molecular dynamics simulation studies of bile, bile salts, lipid-based drug formulations, and mRNA lipid nanoparticles: a review. Mol. Pharmaceut. 20, 2781–2800. https://doi.org/10.1021/acs.molpharmaceut.3c00049.

Hockney, R.W., Goel, S.P., Eastwood, J., 1974. Quiet high resolution computer models of a plasma. J. Comp. Phys. 14, 148–158. https://doi.org/10.1016/0021-9991(74)90010-2.

Hofmann, A., Hagey, L., 2014. Key discoveries in bile acid chemistry and biology and their clinical applications: history of the last eight decades. J. Lipid Res. 55, 1553. https://doi.org/10.1194/jlr.R049437.

Hossain, S., Kneiszl, R., Larsson, P., 2023. Revealing the interaction between peptide drugs and permeation enhancers in the presence of intestinal bile salts. Nanoscale 15, 19180. https://doi.org/10.1039/D3NR05571J.

Humphrey, W., Dalke, A., Schulten, K., 1996. VMD: visual Molecular Dynamics. J. Mol. Graphics 14, 33–38. https://doi.org/10.1016/0263-7855(96)00018-5.

Jorgensen, W.L., Chandrasekhar, J., Madura, J.D., Impey, R.W., Klein, M.L., 1983. Comparison of simple potential functions for simulating liquid water. J. Chem. Phys. 79, 926–935. https://doi.org/10.1063/1.445869.

Kabedev, A., Hossain, S., Hubert, M., Larsson, P., Bergström, C.A.S., 2021. Molecular dynamics simulations reveal membrane interactions for poorly water-soluble drugs: impact of bile solubilization and drug aggregation. J. Pharm. Sci. 110 (1), 176–185. https://doi.org/10.1016/j.xphs.2020.10.061.

Katev, V., Vinarov, Z., Tcholakova, S., 2021. Mechanisms of drug solubilization by polar lipids in biorelevant media. Eur. J. Pharm. Sci. 159, 105733. https://doi.org/10.1016/j.ejps.2021.105733.

Lindahl, Abraham, Hess, van der Spoel, 2021. GROMACS 2021.3 Manual (2021.3). Zenodo. https://doi.org/10.5281/zenodo.5053220.

Malik, N., 2016. Solubilization and interaction studies of bile salts with surfactants and drugs: a review. *Appl. Biochem. Biotechnol* 179 (2), 179–201. https://doi.org/10.1007/s12010-016-1987-x.

Editor(s): Mantri, R.V., Sanghvi, R., Zhu, H.J, 2017. Chapter 1 - solubility of pharmaceutical solids. In: Qiu, Yihong, Chen, Yisheng, Zhang, Geoff GZ., Yu, Lawrence, Mantri, Rao V. (Eds.), Developing Solid Oral Dosage Forms, 2nd Edition. Academic Press, pp. 3–22. https://doi.org/10.1016/B978-0-12-802447-8.00001-7.

Marrink, S.J., Mark, A.E., 2002. Molecular dynamics simulations of mixed micelles modeling human bile. Biochemistry 41 (17), 5375–5382. https://doi.org/10.1021/bi015613i.

Miyamoto, S., Kollman, P.A., 1992. Settle: an analytical version of the SHAKE and RATTLE algorithm for rigid water models. *J. Comput. Chem.* 13, 952–962. https://doi.org/10.1002/jcc.540130805.

Mu, H., Hoy, C.-E., 2004. The digestion of dietary triacylglycerols. Prog. Lipid Res. 43 (2), 105–133. https://doi.org/10.1016/S0163-7827(03)00050-X.

Mustan, F., Genchev, N., Vinarova, L., Bevernage, J., Tistaert, C., et al., 2025. Understanding drug solubilization in intestinal mixed micelles through molecular dynamics simulations. *J. Coll. Interf. Sci.* 684, 225–234. https://doi.org/10.1016/j.jcis.2025.01.088.

Mustan, F., Ivanova, A., Madjarova, G., Tcholakova, S., Denkov, N., 2015. Molecular dynamics simulation of the aggregation patterns in aqueous solutions of bile salts at physiological conditions. J. Phys. Chem. B 119, 15631–15643. https://doi.org/10.1021/acs.jpcb.5b07063.

Mustan, F., Ivanova, A., Tcholakova, S., 2024. Taurodeoxycholate aggregation explored by molecular dynamics: primary-to-secondary micelle transition and formation of mixed micelles with fatty acids. Molecules 29, 5897. https://doi.org/10.3390/molecules29245897.

Parrow, A., Larsson, P., Augustijns, P., Bergström, C.A.S., 2020. Molecular dynamics simulations on interindividual variability of intestinal fluids: impact on drug solubilization. Mol. Pharmaceutics 17, 3837–3844. https://doi.org/10.1021/acs.molpharmaceut.0c00588.

Parrow, A., Larsson, P., Augustijns, P., Bergstrom, C.A.S., 2023. Molecular dynamics simulations of self-assembling colloids in fed-State Human intestinal fluids and their solubilization of lipophilic drugs. Mol. Pharmaceutics 20, 451–460. https://doi.org/10.1021/acs.molpharmaceut.2c00710.

Pavlovic, N., Golocorbin-Kon, S., Danic, M., Stanimirov, B., Al-Salami, et al., 2018. Bile acids and their derivatives as potential modifiers of drug release and pharmacokinetic profiles. Front. Pharmacol. 9, 1283. https://doi.org/10.3389/fphar.2018.01283.

Phan, S., Salentinig, S., Gilbert, E., Darwish, T., Hawley, A., et al., 2015. Disposition and crystallization of saturated fatty acid in mixed micelles of relevance to lipid digestion. J. Colloid Interface Sci. 449, 160–166. https://doi.org/10.1016/j.jcis.2014.11.026.

Pouton, C.W., 2006. Formulation of poorly water-soluble drugs for oral administration: physicochemical and physiological issues and the lipid formulation classification system. Eur. J. Pharm. Sci. 29 (3–4), 278–287. https://doi.org/10.1016/j.ejps.2006.04.016.

Ryckaert, J.-P., Ciccotti, G., Berendsen, H.J.C., 1977. Numerical integration of the cartesian equations of motion of a system with constraints: molecular dynamics of n-alkanes. *J. Comput. Phys.* 23, 327–341. https://doi.org/10.1016/0021-9991(77)90098-5.

Srivastava, A., Tiwari, S., Hani, U., Begum, M.Y., Azum, N., Rub, M.A., 2026. Micellar synergism of bile salts and octyl glucoside for improved indomethacin and ibuprofen drug binding and solubility. Colloids Surf. A 729, 138922. https://doi.org/10.1016/j.colsurfa.2025.138922.

Tuncer, E., Bayramoglu, B., 2019. Characterization of the self-assembly and size dependent structural properties of dietary mixed micelles by molecular dynamics simulations. *Biophys. Chem.* 248, 16–27. https://doi.org/10.1016/j.bpc.2019.02.001.

Tuncer, E., Bayramoğlu, B., 2022. Molecular dynamics simulations of duodenal self assembly in the presence of different fatty acids. Colloids Surf. A 644, 128866. https://doi.org/10.1016/j.colsurfa.2022.128866.

Xiang, T.-X., Anderson, B.D., 2013. Molecular dynamics simulation of amorphous indomethacin-poly(Vinylpyrrolidone) glasses: solubility and hydrogen bonding interactions. J. Pharm. Sci. 102 (3), 876–891. https://doi.org/10.1002/jps.23353.

Zhu, C., Byrd, R.H., Nocedal, J., 1997. L-BFGS-B: algorithm 778: L-BFGS-B, FORTRAN routines for large scale bound constrained optimization. ACM Trans. *Math. Softw.* 23, 550–560. https://doi.org/10.1145/279232.279236.